

See discussions, stats, and author profiles for this publication at: <https://www.researchgate.net/publication/315370269>

# A Deployable High-Gain Antenna Bound for Mars: Developing a new folded-panel reflectarray for the first CubeSat mission to Mars.

Article in IEEE Antennas and Propagation Magazine · February 2017

DOI: 10.1109/MAP.2017.2655561

---

CITATIONS

7

READS

1,233

4 authors, including:



Nacer Chahat

NASA Jet Propulsion Laboratory

85 PUBLICATIONS 874 CITATIONS

[SEE PROFILE](#)

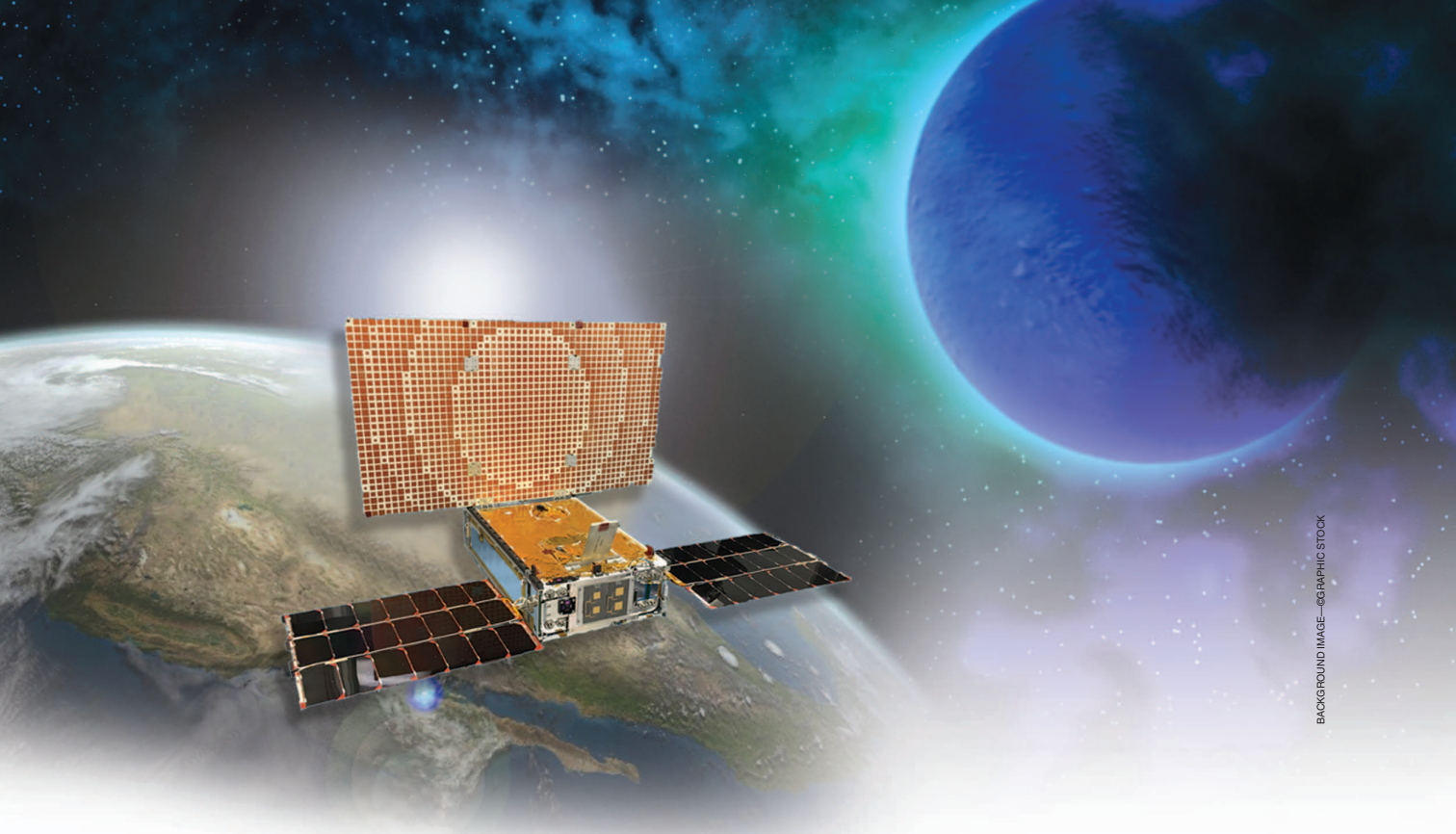
Some of the authors of this publication are also working on these related projects:



Ka-band Parabolic Deployable Antenna (KaPDA) [View project](#)



Tropospheric Water and Cloud Ice (TWICE) [View project](#)



BACKGROUND IMAGE—©GRAPHIC STOCK

# A Deployable High-Gain Antenna Bound for Mars

*Developing a new folded-panel reflectarray for the first CubeSat mission to Mars.*

Richard E. Hodges,  
Nacer Chahat, Daniel J. Hoppe,  
and Joseph D. Vacchione

This article describes the development of a deployable high-gain antenna (HGA) for the proposed Mars Cube One (MarCO) CubeSat mission to Mars. The antenna is a new folded-panel reflectarray (FPR) designed to fit on a 6U ( $10 \times 20 \times 34 \text{ cm}^3$ ) CubeSat bus and support 8.425-GHz Mars-to-Earth telecommunications. The FPR provides a gain of 29.2 dBi with right-hand circular polarization (RHCP). Small stowage volume is a key advantage of the FPR design, as it only consumes ~4% of the usable spacecraft payload volume with a mass of less than 1 kg.

## THE MISSION AND THE ANTENNA

### INTERPLANETARY CUBESATS AND THE MARCO MISSION

CubeSat launches for low-Earth orbit missions have increased dramatically in the last decade due to their low cost, relatively fast

Digital Object Identifier 10.1109/MAP.2017.2655561  
Date of publication: 21 February 2017

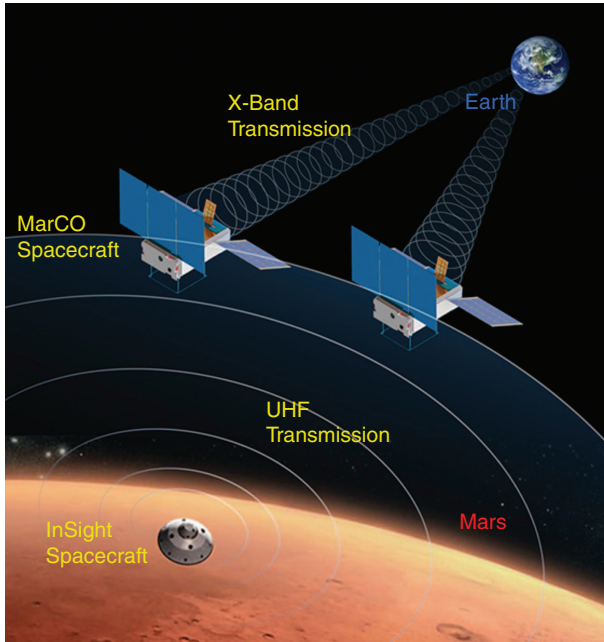


**FIGURE 1.** The MarCO bent-pipe Mars-to-Earth telecommunications relay concept. (Image courtesy of JPL Photographic Services.)

development, and potential to provide unique telecommunications, imaging, and Earth science capabilities. More recently, the advantages offered by CubeSats have gained attention for NASA space exploration missions beyond Earth's orbit. NASA's proposed MarCO mission is among the first missions planned to fly a CubeSat into deep space. NASA plans to launch several additional CubeSats beyond Earth's orbit, including BioSentinel, NEAScout, Lunar Flashlight, and INSPIRE [1], [2]. These missions are targeted for lunar, asteroid, and planetary destinations in which a telecom system must contend with large free-space attenuation to achieve even a relatively low data rate.

The MarCO CubeSats are planned to fly alongside the InSight mission in 2018 and provide a real-time bent-pipe communications link during the entry, descent, and landing (EDL) phase (Figure 1). While InSight could utilize telecommunications satellites orbiting Mars, such as the Mars Reconnaissance Orbiter (MRO), EDL communications force an orbit trim maneuver to adjust the orbit phasing, which consumes propellant and diverts the MRO from its science mission [3]. Moreover, this can cause a delay of several hours in getting EDL landing status data back to Earth. MarCO is expected to provide a new, low-cost method to rapidly retrieve EDL-critical event data. Just as important, MarCO will provide a useful technical demonstration that a CubeSat can perform critical functions in a deep space environment.

MarCO uses twin communications-relay CubeSats built by NASA's Jet Propulsion Laboratory. During EDL, Insight will transmit spacecraft status data on an ultrahigh-frequency (UHF) link at 8 kb/s. Each MarCO CubeSat is designed to receive the EDL data using a deployable, circularly polarized UHF loop antenna. These data are then transmitted via a software-defined radio on an X-band link to a 70-m NASA Deep Space Network antenna at a distance of 1.07 AU (160 million km).

Meeting these communication system requirements in a 6U ( $10 \times 20 \times 34 \text{ cm}^3$ ) CubeSat is a significant challenge for two key reasons: transmit power and antenna gain. The X-band transmit power for most CubeSats is limited to a few watts (~5 W at X-band) due to available solar panel power, thermal management limitations, and radio stowage volume constraints [4]. With a 5-W transmitter and assuming a maximum pointing loss of 3 dB driven by the satellite pointing accuracy of  $\pm 2^\circ$ , the 8-kb/s data rate requires MarCO to be equipped with a 28.0-dBi X-band HGA. This antenna gain is very difficult to achieve due to limited CubeSat stowage volume and mass restrictions.

#### MARCO HGA REQUIREMENTS

The MarCO spacecraft bus configuration must fit in a standard 6U launch canister. In addition to standard CubeSat subsystems such as solar power, avionics, and attitude determination and control systems, the MarCO spacecraft must support the dual-band UHF and X-band telecommunications system and a propulsion system. Moreover,

to achieve the required antenna-pointing accuracy, a reaction wheel system is needed, which occupies a significant fraction of the CubeSat stowage volume [5]. As a result of the need to support these necessary subsystems, there is essentially no volume remaining to stow an HGA.

The key MarCO HGA requirement is a gain of 28 dBi over the 8.400–8.450-GHz downlink frequency band.

As with all CubeSat missions, there are strict mass limitations. MarCO was developed to meet a September 2016 InSight launch and a very aggressive CubeSat development budget. Thus, the challenge was to develop and deliver two flight-qualified antennas that provide the required 28-dBi gain in practically zero stowed volume with less than 2-kg mass at low cost on a strictly enforced one-year, start-to-finish schedule.

Figure 2 provides a summary of antenna options that were considered for the MarCO mission. Although a standard microstrip patch antenna is simple and reliable, a deployable antenna is necessary because the available  $34 \times 20 \text{ cm}^2$  area on the side of the CubeSat is not large enough to hold a patch antenna that can meet the gain requirement. A deployable mesh reflector [6] is not

**NASA's proposed MarCO mission is among the first missions planned to fly a CubeSat into deep space.**

viable due to relatively large stowed volume. In addition, the MarCO mission requires the HGA beam to point  $\sim 23^\circ$  from the spacecraft axis to simultaneously point the UHF antenna toward Mars and the HGA toward Earth. The parabolic reflector antenna does not meet this requirement.

The MarCO antenna design is based on the FPR concept that was originally developed for the Integrated Solar Array and Reflectarray Antenna (ISARA) mission [7]–[9]. Figure 3 illustrates the configuration used to mount an FPR on the MarCO 6U spacecraft bus. The reflectarray is composed of three flat panels that stow by folding flat against the side of the spacecraft. The FPR offers small stowed volume, low mass, and low cost. The simple deployment mechanism is relatively easy to design, which fits the rapid development schedule. This combination of features makes the MarCO reflectarray a mission-enabling technology; without this antenna, there would be no MarCO mission.

We strongly believe the FPR antenna will prove to be a key technology enabling the expanded use of CubeSats in telecommunications and science missions. Whether in low-Earth orbit or in deep space, these missions will require HGAs. The HGA must have a flexible architecture that can be readily adapted to meet unique mission-specific requirements on a tight budget and short schedule. FPR antennas are mechanically simple and relatively easy to configure and adapt to different bus configurations. FPRs also provide the ability to control beam-pointing direction and create shaped beams. The combined advantages of performance, adaptable beamforming, low mass, modest stowage, and low cost make the FPR an excellent antenna for CubeSats.

## FPR ANTENNA DESIGN

### MARCO FPR CONFIGURATION

The MarCO FPR antenna is composed of three  $19.9 \text{ cm} \times 33.5 \text{ cm}$  panels that are attached to one another using spring-loaded hinges as illustrated in Figure 4. At launch, the reflectarray panels are folded down against the spacecraft body with the three reflectarray panels folded against each other to form a single  $19.9 \times 33.5 \times 1.25 \text{ cm}^3$  panel stack [Figure 4(a)]. The arrays are held flush to the spacecraft body using a Vectran tie-down for launch. Shortly after launch, the reflectarray and feed are deployed [Figure 4(b)] using a Nichrome burn wire to sever the Vectran tie-down.

	Patch Array	Reflectarray	Mesh Reflector
Max. Aperture 6U Bus	<b><math>20 \text{ cm} \times 34 \text{ cm}</math> <math>680 \text{ cm}^2</math></b>	$60 \text{ cm} \times 34 \text{ cm}$ $2,040 \text{ cm}^2$	$0.5 \text{ cm Diameter}$ $1,964 \text{ cm}^2$
Gain	<b>24 dB</b>	>28 dB	>28 dB
$23^\circ$ Pointing	Yes	Yes	No
Bandwidth	Medium, < 10%	Low-Medium, < 5%	Large (Feed Limit)
Sidelobes	Controllable	Low	Medium High
Stowage	Small (~0.1 U)	Small (~0.1 U)	Large (~1.5 U)
Deployment Complexity	None	Simple Hinge + Flip-Out Feed	30 Folding Ribs + Deploy Feed and Sub
Reliability	No Deployment	No Lifetime Issues	Mesh Snags, etc.
Mass	Low, <2 kg (est)	Low, <1 kg	Low, 1.4 kg
Cost	Low	Low	Medium

**FIGURE 2.** A trade matrix of MarCO HGA antenna design options.

A  $4 \times 2$  element microstrip patch antenna is used to feed the reflectarray antenna. This feed is mounted on a thin aluminum plate that has a simple spring-loaded hinge and a small rotary joint. The feed folds underneath the reflectarray stack and tucks into a small rectangular pocket in the bus. When commanded to deploy, the FPR panel assembly rotates away from the bus on the root hinge axis, while the two wing panels simultaneously rotate away from the center panel and the feed “flips out” from its stowed position in the bus. The deployment sequence is driven with simple torque springs and is completed within a few seconds. This arrangement offers the advantage that a single release mechanism actuates the entire deployment sequence, which increases reliability.

The FPR offers a considerable stowage advantage because the reflector occupies a very small fraction of the

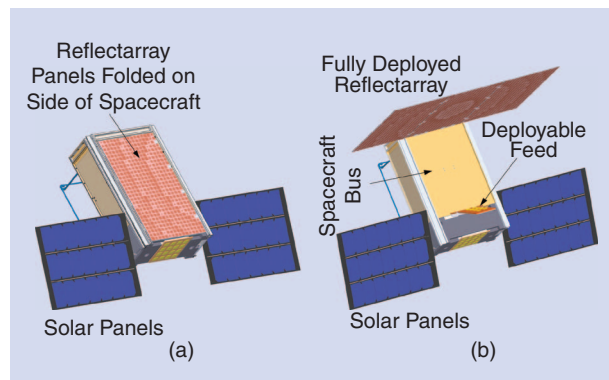


**FIGURE 3.** The MarCO FPR concept: (a) stowed and (b) deployed.

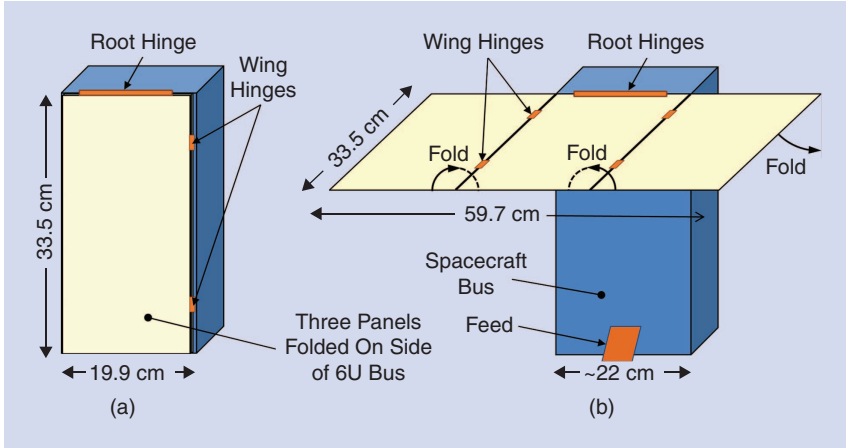


**FIGURE 4.** The MarCO FPR (a) stowed and (b) deployed.

usable space within the bus. A variance in the CubeSat standards that is intended for solar panel stowage allows over 70% of the 12.5-mm depth of the reflectarray assembly to be stowed in the dead space between the outside of the CubeSat bus envelope and the inside wall of the launch canister. Note that a horn or waveguide slot array feed could increase efficiency to ~50%, but this would consume a larger spacecraft volume.

### REFLECTOR OPTICS

Figure 5 shows the MarCO offset-fed reflectarray optics configuration. The feed is mounted on the side of the CubeSat bus. The location is a compromise between the need to maximize focal length (reduce mechanical tolerance sensitivity), simplify the feed design, and minimize the length of the coaxial cable from the radio. The MarCO mission has an additional requirement to point the antenna main beam toward Earth at ~22.6° from the broad face of the spacecraft. A focal length of 31.493 cm provides a nearly ideal solution. Since the specular ray bounce direction is in

the desired beam-pointing direction, it is not necessary to use the reflectarray phase control property to steer the beam, resulting in a very robust antenna design.

It is useful to note that a reflectarray is capable of producing a wide range of beam-pointing directions to meet various system requirements. Specular designs can accommodate an elevation scan range of 0° to at least 30° by adjusting the deployment angle of the reflectarray root hinge. The configuration in Figure 5 has a root hinge angle  $\alpha_r$  of 90°, but it is a simple matter to modify the hinge to stop at a different angle. Additionally, one can

use the reflectarray phase control to steer the beam or alter the beam shape if desired.

### REFLECTARRAY RADIO-FREQUENCY DESIGN

The MarCO antenna uses a variable size square patch microstrip reflectarray design [11]. The required phase of each element is determined from the reflectarray design equation

$$\phi_i + \phi_0 - k_0(R_i + \bar{r}_i \cdot \hat{r}_0) = 2\pi N, \quad (1)$$

where  $R_i$  is the distance from the feed to the  $i$ th array element,  $\phi_i$  is the phase of the field reflected from the  $i$ th element,  $\phi_0$  is an arbitrary phase constant,  $\bar{r}_i$  is a vector from the center of the array to the  $i$ th array element, and  $\hat{r}_0$  is a unit vector in the main beam direction. A unit cell Floquet mode-moment-method technique [12], [13] is used to design the patch artwork and perform radiation pattern calculations. This design methodology assumes that each patch is surrounded by identical patches. Because the MarCO aperture is electrically small for a reflectarray ( $9.4\lambda \times 16.8\lambda$ ), it is advantageous to minimize the element spacing to maximize the number of patches and create a more uniform environment surrounding each patch.

A key goal of the radio-frequency (RF) design is to minimize the dielectric substrate thickness to reduce stowage volume and mass. However, reducing the substrate thickness has the undesirable effect of degrading patch bandwidth and increasing sensitivity to etching tolerance. It has been found that reducing patch element spacing to less than half of a free space wavelength results in increased bandwidth for a fixed substrate thickness [14]. For MarCO, this property is used instead to reduce substrate thickness. Simultaneously reducing substrate thickness and reflectarray element spacing provides a way to achieve the desired antenna depth while maintaining sufficient bandwidth. This has the added advantage of increasing the number of elements, creating a more uniform patch environment that more closely approximates infinite array boundary conditions.

MarCO reflectarray panels are designed with Rogers RO4003 woven glass-reinforced hydrocarbon ceramic

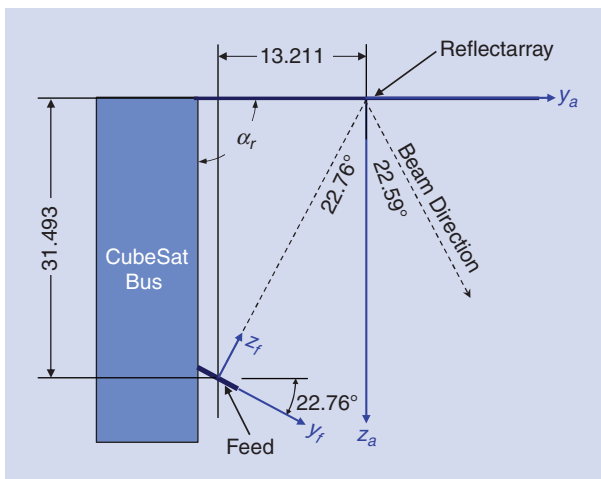


**FIGURE 5.** The MarCO reflectarray antenna optics design and dimensions.

circuit board material. The substrate thickness is 0.812 mm (0.032 in), and the manufacturer's stated dielectric constant is 3.55 with a loss tangent of 0.027. Figure 6 shows the MarCO S-curve design, which gives the reflection phase versus patch size at an incident angle of 23°. The array spacing is 1.168 cm (0.460 in) in the  $x_a$  direction by 1.189 cm (0.468 in) in the  $y_a$  direction. This corresponds to an array spacing of  $\sim 0.33$  wavelengths, which is a good compromise in terms of bandwidth, substrate thickness, and fitting the array lattice to the physical area available for the antenna.

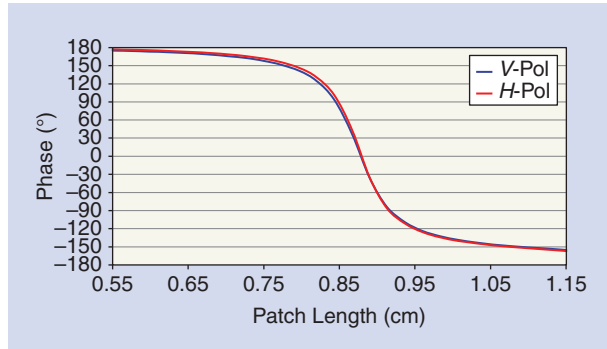
In engineering practice, resonant patches are most sensitive to patch size, dielectric constant, and surrounding environment. For example, in Figure 6 the S-curve phase slope is maximum for patches near resonance (reflection phase of roughly 0°). Conversely, nonresonant patches, which are either a very small or large percentage of a unit cell area (reflection phase of  $\sim \pm 180^\circ$ ) are insensitive to patch size and other physical parameters because the unit cell is essentially just a metallic sheet. This observation suggests that the reflectarray will more closely approximate infinite array boundary conditions, and therefore will perform better, if it is designed to minimize the number of resonant patches that are located near discontinuities such as edges, panel fold lines, hinges, etc. This is accomplished by adjusting the arbitrary phase constant  $\phi_0$  in (1), which controls the location of phase wrap rings.

Figure 7 illustrates this point with two MarCO reflectarray designs corresponding to  $\phi_0 = 80^\circ$  and  $\phi_0 = 240^\circ$ . The figure illustrates reflectarray patches in an array that is sized to fit the three MarCO panels. In Figure 7(a), the central phase wrap ring is relatively small and fully contained within the center panel, while in Figure 7(b) the center ring is much larger. As the phase constant  $\phi_0$  increases from  $80^\circ$  to  $240^\circ$ , the diameter of the phase wrap rings monotonically increase. It is found that the computed antenna directivity, beamwidth, and sidelobes are remarkably insensitive to changes in the phase parameter  $\phi_0$ . Consequently, one can adjust  $\phi_0$  to minimize the number of resonant patches located near discontinuities without otherwise compromising antenna performance.

Figure 7(b) shows the final MarCO design, which is composed of three  $17 \times 28$  reflectarray patch arrays. The figure also includes symbols that indicate the location of physical features on the panels. The red rectangles represent hinge parts and panel cutouts, vertical black lines indicate hinge fold lines, and red circles are alignment and stowage features. Note that the phase wrap ring locations have been adjusted to align with the edges of the array, hinges, hinge fold lines, and other discontinuities to minimize the effect on resonant patches. In contrast, the design in Figure 7(a) was rejected because the wing hinges are located in a resonant patch region, and a large percentage of patches along the hinge fold are resonant.

### REFLECTARRAY PANEL PHYSICAL DESIGN

The MarCO antenna must survive the launch vibration environment and maintain panel flatness over a range of temperatures. The key to meet this requirement is a stiff, rugged



**FIGURE 6.** The MarCO reflectarray S-curve of reflection phase versus patch size.

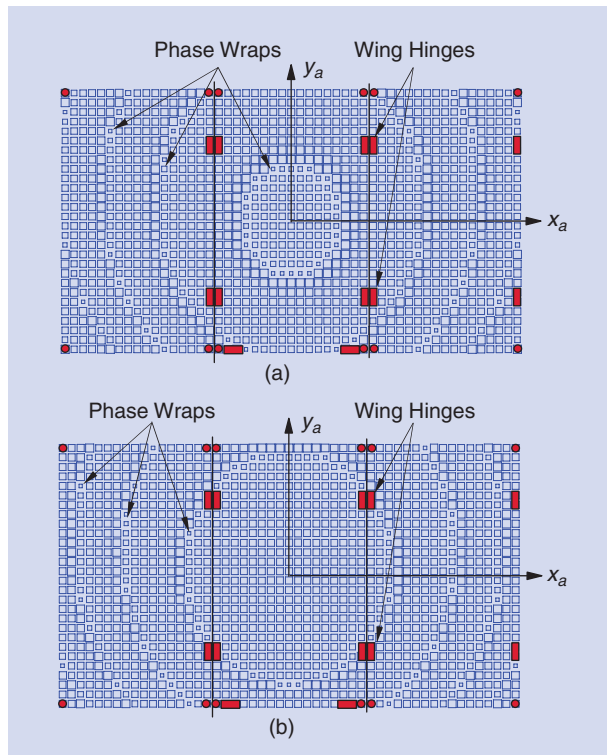


**FIGURE 7.** Two reflectarray designs based on two values of arbitrary phase constant: (a)  $\phi_0 = 80^\circ$  (rejected design) and (b)  $\phi_0 = 240^\circ$  (final design).

panel material that has good RF dielectric properties and good thermal continuity to minimize bowing effects. A new material was developed to meet this need. The construction concept is similar to panels developed for ISARA [7]–[9].

The MarCO panel layer thicknesses and material properties, described in Figure 8, are based on thermal models that predict temperature gradients through the material along with structural finite element method analysis to predict panel deformation. The Rogers RO4003 woven glass-reinforced hydrocarbon ceramic circuit board provides good RF performance and panel stiffness. The sandwich structure also uses an epoxy matrix composite material developed by STABLCOR [15] with

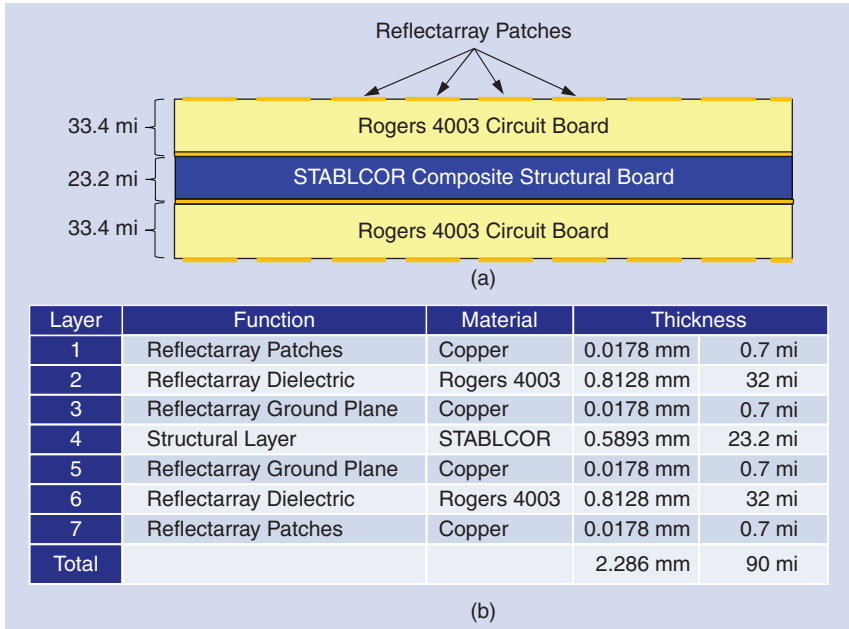


**FIGURE 8.** MarCO reflectarray panel construction details: (a) a panel circuit board cross section and (b) a table of layer materials and thicknesses.

Nippon XN-80-60S carbon fibers for high strength, good thermal conductivity, and a low coefficient of thermal expansion. The physical symmetry of the panel cross section is required to eliminate panel bow caused by bulk temperature effects. Note that the reflectarray patch pattern is duplicated on both sides of the panel to maintain symmetry.

The sandwich structure is fabricated using a co-cure process in which the STABLCOR material is cured in an autoclave together with the RO4003 sheets. This process simultaneously cures the STABLCOR and bonds the RO4003 panels in a single step, thereby eliminating the need for an additional adhesive layer. The result is a very flat, durable, thermally stable panel with minimal thickness and high strength. The reflectarray patch pattern is photoetched after the co-cure process is complete to provide the most accurate imaging.

#### PANEL DEPLOYMENT MECHANISM

The panel deployment mechanism consists of the following components: 1) root hinge, 2) four wing hinges, and 3) a burn wire release mechanism. Although the detailed mechanical design of the deployment mechanism components is beyond the scope of this article, we provide a general description of the components and characteristics that are relevant to RF performance.

**Simultaneously  
reducing substrate  
thickness and  
reflectarray element  
spacing provides a way  
to achieve the desired  
antenna depth while  
maintaining sufficient  
bandwidth.**

From an antenna performance perspective, the most important components are hinges because they largely control deployment accuracy and repeatability. As discussed later, the root hinge primarily affects beam pointing and otherwise has very little impact on the antenna performance, while the wing hinges can significantly influence both gain and beam pointing.

Antenna stowage volume is the key constraint that drives MarCO hinge design because the hinge stack height determines the total depth of the folded panel assembly. Simple torsion spring-actuated butt hinges are used for the wing deployment, and a torsion spring-actuated offset design is used for the root hinge. The hinges use U-shaped channels that wrap around the circuit boards to minimize stowed panel thickness. A bonding process known as liquid shim is used to attach the hinges to the panels. In this pro-

cess, the deployed panel assembly is aligned in a tooling jig, and adhesive is injected into the small gaps between the

U-shaped channel and the panel material. This technique enables a simple, low-cost hinge to provide highly accurate and repeatable panel deployment. However, it was found that the bond material can soften in thermal cycles. The stowed spring force can then cause the panels to move within the hinge, resulting in a small fixed-deployment error. To prevent this, small wires are inserted prior to injection to reinforce the liquid shim material.

The panel assembly was measured using a photogrammetry system to estimate panel flatness, deployment angle, and repeatability. Root mean square (rms) surface flatness was found to be ~0.95 mm. The maximum wing deployment angle error measured in five trials was 0.27° for +X panel and 0.08° for the -X panel. The larger deployment error of the +X panel is believed to be due to hinge bond settling. The sample standard deviation after five deployments was 0.017° and 0.037°. Root hinge deployment results showed a maximum error of ~0.02° for the overall best fit plane and <0.20° for an individual panel, with a sample standard deviation of 0.011°. Plots of the panel surface photogrammetry data indicated that the overall panel has a slight twist deformation. All of these repeatability values are well within acceptable limits.

## FEED DESIGN AND PERFORMANCE

### FEED ANTENNA DESIGN

The circularly polarized MarCO feed is a key component that drives the HGA performance: 1) minimizes taper and spillover loss affecting the antenna directivity, 2) controls the cross-polarization discrimination, and 3) mitigates multipath interference from the CubeSat bus. The feed is a  $4 \times 2$  element microstrip patch array designed to create edge taper of approximately  $-10$  dB. The edge taper angle is set by the reflectarray antenna optics design (Figure 5). A  $-10$ -dB beamwidth of  $47.1 \pm 2^\circ$  in elevation and  $84.1 \pm 2^\circ$  in azimuth is required to minimize spillover and taper loss.

The reflectarray circular polarization is formed by the feed patch array design, while the reflectarray itself is a dual linearly polarized design. As RHCP is targeted, the feed is left-hand circularly polarized. Maintaining good cross-pole performance over the frequency band proved to be a significant challenge.

Figure 9 illustrates the  $4 \times 2$  element microstrip patch array and corporate feed circuit board layout. The feed assembly is approximately  $9.2 \times 4.2$  cm with a depth of 4.7 mm. To minimize fabrication complexity, corner-truncated patches are used to generate left-hand circular polarization (LHCP). To avoid any spurious radiation generated by corporate feed lines, the antenna utilizes a probe-fed patch element excited by a stripline corporate feed [Figure 9(b)]. The design uses Rogers 6002 board material, with a nominal dielectric constant of 2.94 and a loss tangent of 0.0012. The patch substrate thickness is 0.762 mm (0.030 in), while the stripline board has a total thickness of 3.048 mm (0.120 in). Via fences are used to eliminate stripline cross-coupling issues.

In addition, the sidelobe levels (SLL) in the direction of the CubeSat bus must be controlled and minimized. Analysis performed on TICRA GRASP using physical optics shows that the SLL should be  $<-20$  dB to avoid multipath issues. Therefore, a  $-20$ -dB Taylor distribution is used [Figure 9(b)]. This also reduces spillover loss. Note that each patch is excited perpendicularly to the elevation plane,

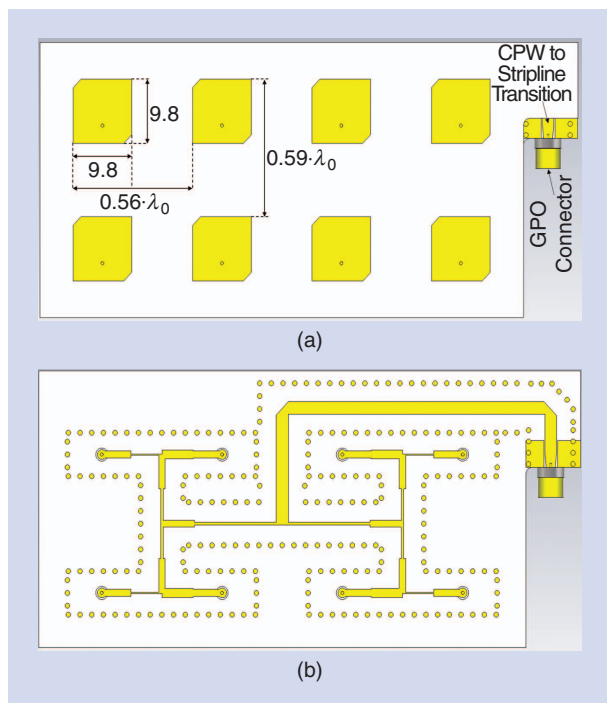


**FIGURE 9.** A microstrip patch antenna array model: (a) the top layer and (b) the stripline corporate feed used to generate Taylor distribution.

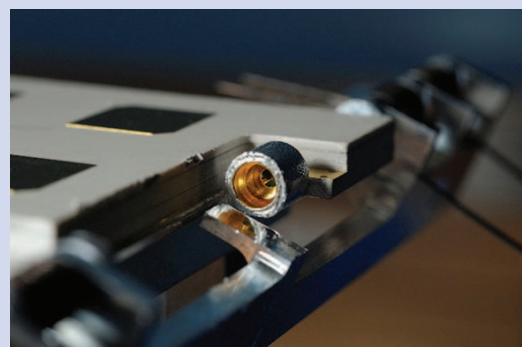
which causes an asymmetry in the SLL. This results in additional SLL reduction on one side of the feed, which essentially eliminates multipath interference.

### FEED MOUNTING AND DEPLOYMENT MECHANISM

The feed and the shroud connector are bonded to aluminum plates using a conductive epoxy. This plate is attached to a spring-loaded hinge to provide the “flip-out” deployment mechanism [Figure 10(a)]. As noted earlier, the feed is restrained in its stowed position by the reflectarray panels and deploys automatically when the panels deploy. A GPO connector is used as a rotary joint [Figure 10(b)]. While not designed for this purpose,



(a)



(b)

**FIGURE 10.** (a) The HGA feed and (b) the GPO rotary joint.

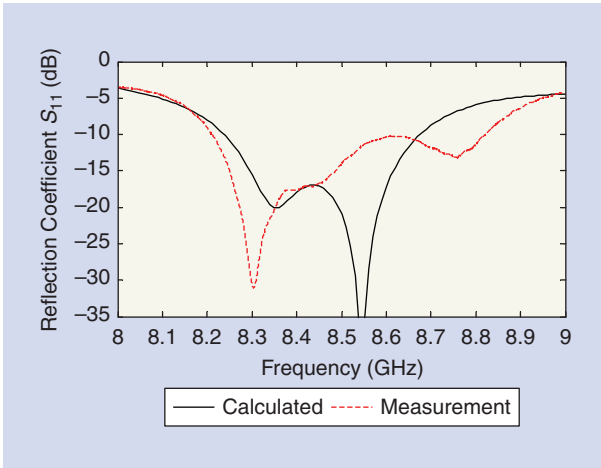


**FIGURE 11.** The reflection coefficient of the reflectarray feed.

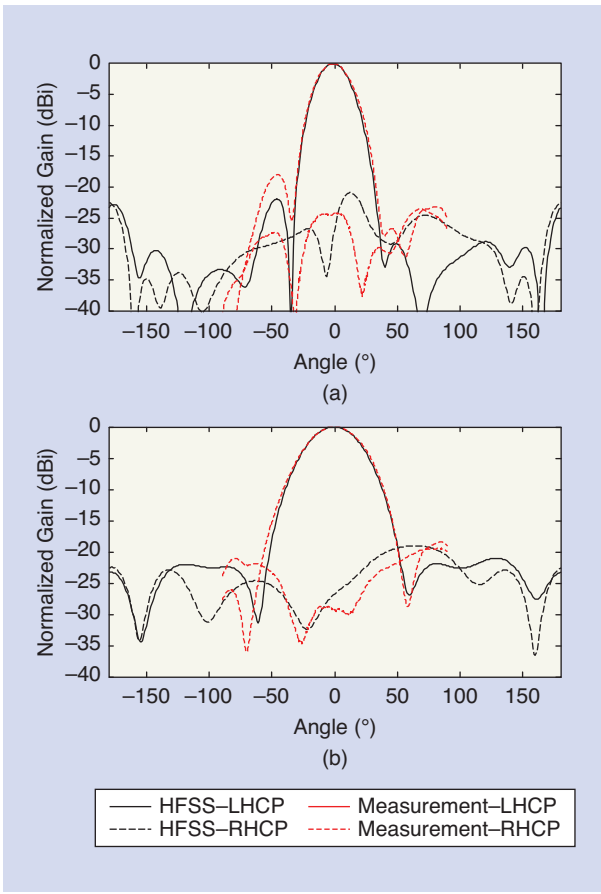


**FIGURE 12.** The feed radiation patterns at 8.425 GHz: (a) the azimuth and (b) the elevation. HFSS: high-frequency structure simulator.

the GPO rotates smoothly and easily and has sufficient lifetime to support deployment testing. The GPO rotary joint offers the advantages of low insertion loss, fit into the hinge space available, low cost, and ready availability.

The GPO connects to a coplanar waveguide (CPW) line [Figure 9(a)]. A CPW-to-stripline transition is optimized

		Frequency (MHz)		
Feed S/N	Reflectarray S/N	8,400	8,425	8,450
S/N 001	N/A	13.59	13.56	13.68
S/N 002	S/N 002	13.84	13.77	13.80
S/N 003	S/N 001	13.82	13.77	13.81

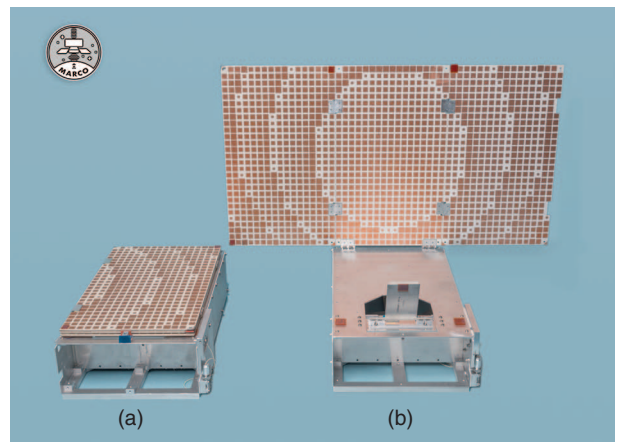


**FIGURE 13.** The MarCO FM antenna mounted on a test bus: (a) stowed and (b) deployed. (Photos courtesy of JPL Photographic Services.)

to minimize the insertion loss ( $\sim 0.1$  dB). The reference point for all measurements (i.e., reflection coefficient and radiation patterns) is taken at the end of the 4-cm coaxial cable [Figure 10(a)]. The measured insertion loss in this cable equals 0.25 dB. Measurements show that the rotation around the GPO shroud does not affect the reflection coefficient or antenna gain.

### FEED PERFORMANCE

The reflection coefficient is optimized to be  $<-15$  dB over the extended frequency band of 8.3–8.5 GHz to compensate for coefficient of thermal expansion over temperatures ranging from  $-55^\circ\text{C}$  to  $+80^\circ\text{C}$ . Figure 11 shows the measured and simulated reflection coefficients. The measured value is  $<-10$  dB from 8.20 to 8.82 GHz.

Figure 12 shows the measured and calculated feed radiation patterns at 8.425 GHz, which are in good agreement. Although not shown, the patterns are nearly identical over the 8.400–8.450-GHz frequency band. Table 1 shows the gain for the three flight model feeds as measured by substitution method using a standard gain horn. The predicted feed circuit loss is 0.74 dB. Both gain and circuit loss measurements agree with predicted values to within  $\sim 0.1$  dB. The axial ratio is  $<1.5$  dB over the frequency band, assuring the MarCO antenna will have low polarization mismatch loss.

The feed assembly also successfully passed deployment tests, thermal cycling, and vibration tests. The deployment mechanism achieved the required angle of  $22.76^\circ \pm 0.2^\circ$  with a repeatability error  $<0.08^\circ$ , which ensures that the desired reflectarray spillover efficiency will be met.

## MARCO FLIGHT MODEL REFLECTARRAY ANTENNA

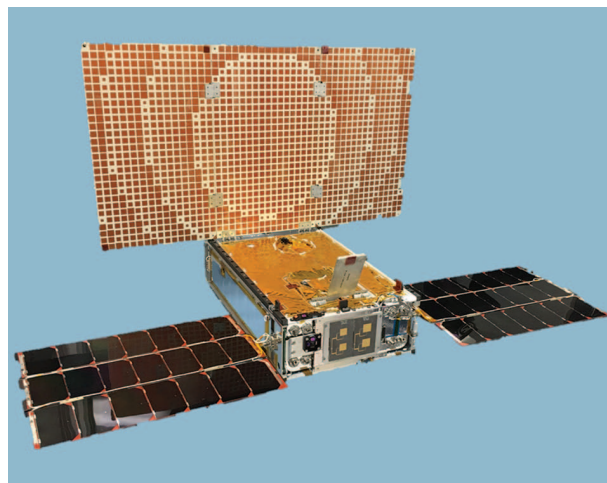
### DESCRIPTION OF FLIGHT MODEL REFLECTARRAY

Figure 13 shows a photograph of the flight model (FM) MarCO reflectarray and feed mounted on a faux bus that was used to perform antenna deployment and radiation pattern tests. The flat stowage property and low profile hinges are visible in the photo. Figure 14 shows the FM antenna mounted on the flight spacecraft. Note the multilayer insulation on the side of the bus presents an irregular scattering surface.

Table 2 gives the gain budget for the two FM MarCO antennas. The computed directivity is slightly different for the two antennas because this calculation is based on measured best-fit reflector plane and feed position. These data indicate that good fabrication repeatability has been achieved. Hinge loss is estimated as the gain penalty on the basis of effective area loss from the hinges and other features in Figures 7 and 13. The computed spillover loss is 1.51 dB, and taper loss is 0.98 dB. The predicted MarCO antenna gain gives an aperture efficiency of 41.6%.

For the flight antennas it is important to estimate the expected gain penalty caused by environmental factors and non-ideal deployment. An extensive tolerance analysis study was performed for this purpose.

Figure 15 presents a semiquantitative summary of the tolerance study results. Red, yellow, and green color coding indicates the relative importance of the various physical parameters and does not indicate a deficiency in the MarCO



**FIGURE 14.** The MarCO S/N 001 antenna mounted on flight spacecraft.

**TABLE 2. MARCO FLIGHT ANTENNAS GAIN BUDGET.**

	S/N 001	S/N 002
<b>Computed directivity</b>	<b>30.56</b>	<b>30.50</b>
Feed loss	-0.74	-0.74
Patch dielectric loss	-0.25	-0.25
Patch conductor loss	-0.04	-0.04
Mismatch loss	-0.14	-0.14
Hinge mounting area loss	-0.15	-0.15
<b>Total loss</b>	<b>-1.32</b>	<b>-1.32</b>
<b>GAIN predict</b>	<b>29.24</b>	<b>29.18</b>

	Gain Impact	Beam Pointing Impact
RMS Surface Error	Quadratic: 1 mm = 0.5 dB	Very Small
Quadratic Bow Surface Error	Quadratic: 2.5 mm = 0.3 dB	None (Asymmetric Not Done)
Root Hinge Angle Error	Nonlinear: $1^\circ = 0.03$ dB	Linear: $1.75^\circ/\text{deg}$
Root Hinge Slip Error	Quadratic: 10 mm = 0.03 dB	Linear: $0.14^\circ/\text{mm}$
Feed Hinge Angle Error	Nonlinear: $1^\circ = 0.04$ dB	Zero
Feed Hinge Slip Error	Quadratic: 10 mm ~0.02 dB	Linear: $0.14^\circ/\text{mm}$
Feed Defocus Error	Quadratic: 25 mm ~0.5 dB	Zero
Wing Hinge Angle Symmetric	Quadratic: $1^\circ \sim 0.08$ dB	Linear: $0.80^\circ/\text{deg}$
Wing Hinge Angle Asymmetric	Quadratic: $1^\circ = 0.35$ dB	Zero
Wing Hinge Slip Symmetric	Quadratic: 10 mm ~0.17 dB	Linear: $0.07^\circ/\text{mm}$
Wing Hinge Slip Asymmetric	Quadratic: 10 mm ~0.27 dB	Linear: $0.02^\circ/\text{mm}$

**FIGURE 15.** The MarCO antenna tolerance study results. Red cells indicate high sensitivity parameters, and green indicates very insensitive parameters. The terms *linear*, *quadratic*, and *nonlinear* describe the shape of the tolerance curves.

**TABLE 3. MARCO REFLECTARRAY ANTENNA RF PERFORMANCE SUMMARY.**

	S/N 001		S/N 002	
	Predict	Meas. (fc)	Predict	Meas. (fc)
Gain (dBiC)	29.2	29.2	29.2	28.8
Polarization	RHCP	RHCP	RHCP	RHCP
Beam pointing	AZ	-0.06°	0.10°	0.45°
	EL	22.53°	22.15°	23.30°
Beamwidth	AZ	3.83°	3.95°	3.82°
	EL	6.97°	6.91°	7.01°
Peak SLL (dB)	AZ	-26.7 dB	-22.6 dB	-26.8 dB
	EL	-21.8 dB	-19.9 dB	-21.0 dB
XPD (dB)	AZ	19.1	20.1	18.7
	EL	27.9	21.0	25.0

AZ: azimuth; EL: elevation; XPD: cross-polarization discrimination; fc: center frequency (8.425 GHz).

antenna. The tolerance study reveals that gain is primarily determined by surface flatness and wing hinge deployment accuracy. Because gain is the key driving requirement, the design team focused attention in these areas. Beam pointing is of secondary importance because the spacecraft can do a search for the beam in transit to Mars. The measured 0.95-mm rms surface deformation is a slow “twist” variation similar to a surface bow distortion; we did not find a noticeable gain loss in the measured data. The important conclusion is that, on the basis of analysis and test data, we believe the MarCO antenna will meet gain requirements in flight.

The final flight configuration shown in Figure 14 meets all physical requirements to fit within the 6U launch canister. The measured mass of the reflectarray panel assembly is 931 g, the feed is 57 g, and the launch release mechanism is 10 g; the total mass of the reflector payload is just under 1 kg.

#### MARCO REFLECTARRAY RF PERFORMANCE SUMMARY

Table 3 gives a summary of the key MarCO antenna RF performance characteristics. The measured performance shows good agreement with predictions and meets all mission requirements. Of greatest importance is the 28-dBiC gain requirement, which has been met with ample margin to allow for measurement error and in-flight thermal distortion. The feed model in this calculation is a spherical wave expansion based on analysis with ANSYS HFSS software. However, the measured feed gain was used in place of the theoretical value.

Note that the predicted values in Table 3 are based on measured feed position and rotation obtained from metrology data, which were incorporated into Jet Propulsion Laboratory reflectarray analysis code. Photogrammetry measurements indicate that the reflector surface has a small nonlinear distortion. For example, data for S/N 001 have a roughly 1-mm “twist” distortion. We believe the small gain discrepancy on S/N 002 is due to a bad cable in the antenna range that was discovered after the test was completed. The measured directivity of the breadboard unit and both flight units is essentially identical. Performance is essentially unchanged over the 50-MHz frequency band.

Figure 16 shows the calculated and measured radiation patterns for the MarCO FM antenna S/N 001; the S/N 002 patterns are essentially identical. These patterns are calculated with a simple array factor summation in which the element excitation is determined by infinite array moment method analysis. The calculation assumes that the entire surface of the reflector is populated with patches; it does not account for patches that were removed to accommodate hinges, cut-outs, alignment features, etc. Scattering from the spacecraft bus and feed is also neglected. Even with all of these

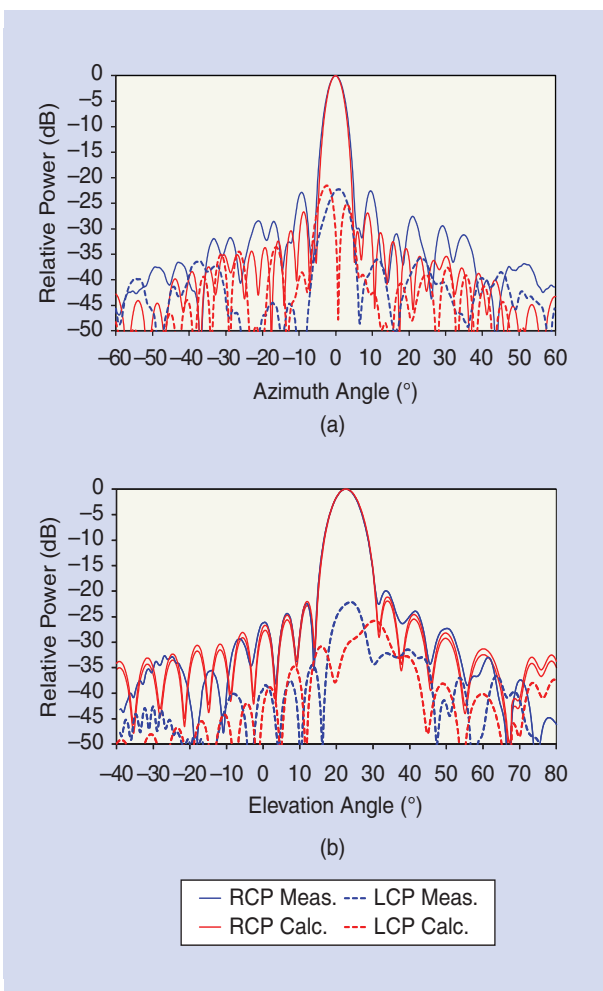


**FIGURE 16.** The MarCO FM reflectarray radiation patterns, 8.425 GHz: (a) the azimuth and (b) the elevation.

approximations, there is good overall agreement between the calculated and measured patterns. This is significant because it suggests that the antenna performance is robust and insensitive to the spacecraft environment.

## CONCLUSIONS

The MarCO spacecraft development shows the potential for CubeSats to play a significant role in deep space missions. HGAs are an essential enabling component for high-data-rate communications or science instruments such as radar, but stowage volume is a fundamental limiting factor because highly capable spacecraft must package a large number of subsystems (avionics, propulsion, power, payload, etc.) into a small volume. Moreover, the CubeSat paradigm of rapid development of unique, specialized spacecraft requires a versatile antenna design that is readily adaptable to meet special requirements for specific missions. The MarCO antenna development demonstrates that the FPR can meet these demands.

The MarCO X-band HGA uses simple spring-loaded hinges to fold into a package just 1.25-cm thick, which is ~12% of the CubeSat payload volume. However, the stowed antenna uses only ~4% of the payload volume because ~70% of it is stowed in the dead space between the outside of the bus and the sides of the launch canister. The measured gain of the FM MarCO antenna is 29.2 dBiC at 8.425 GHz, an efficiency of ~42%. This performance is good considering the low mass (<1 kg) and stowed volume.

## ACKNOWLEDGMENTS

We gratefully acknowledge our colleagues at NASA's Jet Propulsion Laboratory who contributed to this work. Long Chen performed structural analysis and contributed to the design of the panel composite material. Eric Sunada performed thermal analysis of the composite materials. Vinh Bach, Jonathan Sauder, and Phil Walkemeyer developed the deployment mechanism. We also thank Dr. Jefferson Harrell for performing the radiation pattern measurement. The work described in this article was carried out at the Jet Propulsion Laboratory, California Institute of Technology, under a contract with NASA.

## AUTHOR INFORMATION

**Richard E. Hodges** (richard.e.hodges@jpl.nasa.gov) is the supervisor of the Spacecraft Antennas Group and principal engineer at the Jet Propulsion Laboratory in Pasadena, California. His current research interests include spaceborne deployable reflectarray antennas, deployable reflectors, and waveguide slot array antennas. He is a Senior Member of the IEEE.

**Nacer Chahat** (nacer.e.chahat@jpl.nasa.gov) is a senior antenna/microwave engineer with the Jet Propulsion Laboratory in Pasadena, California. His current research fields are deployable antennas for CubeSat, spacecraft antennas for telecommunications, radar, imaging systems, comple-

mentary metal–oxide–semiconductor antennas for space instruments, and wearable antennas. He is a Senior Member of the IEEE.

**Daniel J. Hoppe** (daniel.j.hoppe@jpl.nasa.gov) is a principal engineer at the Jet Propulsion Laboratory (JPL) in Pasadena, California. His work at JPL involves electromagnetic analysis and design of microwave and optical devices for both ground-based and space-based applications. He is a Senior Member of the IEEE.

**Joseph D. Vacchione** (joseph.d.vacchione@jpl.nasa.gov) is a senior engineer at the Jet Propulsion Laboratory in Pasadena, California. He has contributed to and led antenna development teams for numerous Jet Propulsion Laboratory–NASA missions, including Mars Pathfinder, Mars Exploration Rover, Shuttle Radar Topography Mission, Mars Reconnaissance Orbiter, Aquarius Instrument, Juno Telecommunications, and GRACE Follow-On. He is a Member of the IEEE.

## REFERENCES

- [1] National Aeronautics and Space Administration. Biosentinel. [Online]. Available: [www.nasa.gov/centers/ames/engineering/projects/biosentinel.html](http://www.nasa.gov/centers/ames/engineering/projects/biosentinel.html)
- [2] Jet Propulsion Lab. CubeSat missions. [Online]. Available: <http://www.jpl.nasa.gov/cubesat/missions>
- [3] J. Taylor, D. K. Lee, and S. Shambayati. (2006, Sept.). Mars reconnaissance orbiter telecommunications. Jet Propulsion Lab California Inst. Technol. Pasadena, CA. [Online]. Available: [http://descanso.jpl.nasa.gov/DPSummary/MRO\\_092106.pdf](http://descanso.jpl.nasa.gov/DPSummary/MRO_092106.pdf)
- [4] C. B. Duncan, A. E. Smith, and F. H. Aguirre, "Iris transponder: Communications and navigation for deep space," in *Proc. 28th Annu. Amer. Inst. Aeronautics and Astronautics/Utah State University Conf. Small Satellites*, Logan, UT, 2014.
- [5] S. Palo, G. Stafford, A. Hoskins, "An agile multi-use nano star camera for constellation applications," in *Proc. 27th AIAA/USU Conf. Small Satellite Constellations*, Logan, UT, 2013. [Online]. Available: <http://digitalcommons.usu.edu/cgi/viewcontent.cgi?article=292&context=smallsat>
- [6] N. Chahat, J. Sauder, M. Thomson, R. Hodges, and Y. Rahmat-Samii, "CubeSat deployable Ka-band reflector antenna development for Earth science missions," *IEEE Trans. Antennas Propag.*, vol. 64, no. 6, pp. 2083–2093, June 2016.
- [7] R. Hodges, B. Shah, D. Muthulingham, and T. Freeman, "ISARA: Integrated solar array and reflectarray mission overview," in *Proc. Small Satellite Conf. Workshop*, 2013. [Online]. Available: <http://digitalcommons.usu.edu/smallsat/2013/all2013/12/>
- [8] R. E. Hodges, M. J. Radway, A. Toorian, D. J. Hoppe, B. Shah, A. E. Kalman, "ISARA: Integrated solar array and reflectarray antenna CubeSat deployable Ka-band antenna," in *Proc. 2015 Antennas and Propagation Society Int. Symp.*, Vancouver, BC, Canada, 2015, pp. 2141–2142.
- [9] R. Hodges, D. Hoppe, M. Radway, and N. Chahat, "Novel deployable reflectarray antennas for CubeSat communications (*Invited*)," in *Proc. IEEE Microwave Theory and Techniques Society Int. Microwave Symp.*, Phoenix, AZ, 2015.
- [10] J. Huang and J. Encinar, *Reflectarray Antennas*. Hoboken, NJ: Wiley, 2007.
- [11] D. M. Pozar and T. A. Metzler, "Analysis of a reflectarray antenna using microstrip patches of variable size," *Electronics Letters*, vol. 29, no. 8, pp. 657–658, Apr. 1993.
- [12] D. M. Pozar and S. D. Targonski Syrigos, "Design of millimeter wave microstrip reflectarrays," *IEEE Trans. Antennas Propag.*, vol. 45, no. 2, pp. 287–296, Feb. 1997.
- [13] S. R. Rengarajan, *IEEE Antennas and Wireless Propagation Letters*, vol. 4, no. 1, pp. 47–50, June 2005.
- [14] D. M. Pozar, "Wideband reflectarrays using artificial impedance surfaces," *Electronics Lett.*, vol. 43, no. 3, pp. 148–149, Feb. 2007.
- [15] Stablecor Technology, Inc. [Online]. Available: <http://www.stablecor.com>

